On the new vortex shedding mode past a rotating circular cylinder

D. Stojković, P. Schön, M. Breuer, and F. Durst

Citation: Phys. Fluids **15**, 1257 (2003); doi: 10.1063/1.1562940
View online: http://dx.doi.org/10.1063/1.1562940
View Table of Contents: http://pof.aip.org/resource/1/PHFLE6/v15/i5
Published by the AIP Publishing LLC.

On the new vortex shedding mode past a rotating circular cylinder

D. Stojković, P. Schön, M. Breuer,[a] and F. Durst
Institute of Fluid Mechanics, Friedrich–Alexander–Universität Erlangen–Nürnberg, Cauerstraße 4, D-91058 Erlangen, Germany

(Received 2 December 2002; accepted 31 January 2003; published 3 April 2003)

To examine in detail the behavior of a new vortex shedding mode found in a previous investigation [Phys. Fluids **14**, 3160 (2002)], a two-dimensional numerical study on the laminar incompressible flow past a rotating circular cylinder in the Reynolds number range $60 \leqslant \mathrm{Re} \leqslant 200$ and at rotational rates $0 \leqslant \alpha \leqslant 6$ was carried out. The results obtained clearly confirm the existence of the second shedding mode for the entire Reynolds number range investigated. A complete bifurcation diagram $\alpha(\mathrm{Re})$ was compiled defining both kind of shedding modes. The unsteady periodic flow in the second mode is characterized by a frequency much lower than that known for classical von Kármán vortex shedding of the first mode. The corresponding Strouhal number shows a strong dependence on the rotational velocity of the cylinder, while only a weak dependence is observed for the Reynolds number. Furthermore, the amplitudes of the fluctuating lift and drag coefficients are much larger than those characterizing classical vortex shedding behind nonrotating or slowly rotating cylinders. Additionally, negative values for the mean drag denoting thrust are found within the second shedding mode. © *2003 American Institute of Physics.* [DOI: 10.1063/1.1562940]

I. INTRODUCTION

The objective of this brief paper is to present the results of a detailed numerical study on the laminar unsteady periodic flow motion found in the wake of rotating circular cylinders at high rotational velocities.[1] This vortex shedding is characterized by frequencies much lower than that known for normal vortex shedding, i.e., the von Kármán vortex street.[2]

The rotating circular cylinder, placed in a free incompressible fluid flow of constant velocity, is considered. This type of flow is defined by two dimensionless parameters: the Reynolds number $\mathrm{Re}=(U_\infty D)/\nu$ and the ratio of the rotational velocity of the cylinder wall to the oncoming flow velocity $\alpha=(D\,\omega)/(2\,U_\infty)$, where D is the cylinder diameter, ω the constant angular velocity of the cylinder rotation, U_∞ the oncoming free-stream velocity and ν the kinematic viscosity of the fluid.

Recent numerical investigations for the laminar 2D vortex shedding regime performed by Kang *et al.*[3] for $\mathrm{Re}=60$, 100, and 160 and $0 \leqslant \alpha \leqslant 2.5$ showed that vortex shedding exists for $\alpha \leqslant \alpha_\mathrm{I}$, where α_I is the critical rotational velocity, which is a nonlinear function of Re. For the same range of Reynolds numbers and higher rotational rates $\alpha_\mathrm{I} \leqslant \alpha \leqslant 2.5$ vortex shedding disappears. It was shown by Kang *et al.*[3] that the rotation of the cylinder does not significantly alter the Strouhal number St for the range $\alpha \leqslant \alpha_\mathrm{I}$. Actually, St stays nearly constant at lower rotational rates α, decreases slightly as α approaches α_I, and sharply reduces to zero at $\alpha=\alpha_\mathrm{I}$. These results confirmed the assumption of Badr *et al.*[4] that St is more or less independent of α. Furthermore, Kang *et al.*[3] found that the lift force mostly results from the pressure force and its contribution increases with increasing α. The total lift coefficient c_L is almost independent of Re and increases linearly with increasing the rotational rate. The drag coefficient c_D has a relatively strong dependence on Re and α. As Re increases, the drag coefficient decreases. As α increases, the pressure drag decreases while the friction drag increases, resulting in a net decrease in the total drag force.

Stojković *et al.*[1] examined the unsteady flow for $\mathrm{Re}=100$ and high rotational rates $0 \leqslant \alpha \leqslant 12$. They confirmed the results of Kang *et al.*[3] about the existence of vortex shedding for $\mathrm{Re}=100$ and $0 \leqslant \alpha \leqslant \alpha_\mathrm{I}(\mathrm{Re}) \approx 1.8$ and its suppression for $\alpha \geqslant \alpha_\mathrm{I}$. They found that the lift force increases linearly only for lower rotational rates. For $\alpha \geqslant 2$, the mean lift coefficient shows a parabolic increase with α up to $\alpha \leqslant 5.15$. Furthermore, on increasing the rotation rate to even higher values, a second shedding mode was found for a narrow range, $\alpha_\mathrm{II} \leqslant \alpha \leqslant \alpha_\mathrm{III}$, where $\alpha_\mathrm{II}=4.8$ and $\alpha_\mathrm{III}=5.15$ at $\mathrm{Re}=100$. In this range of rotational rates the flow field again shows unsteady behavior. The corresponding Strouhal number was observed to be much lower than that known for the normal shedding mode. For example, in case of $\mathrm{Re}=100$ and $\alpha=5$, $\mathrm{St} \approx 0.022$ was found. Furthermore, the amplitudes of the drag and lift forces were detected to be significantly larger than those characterizing the first shedding mode at $\alpha \leqslant 1.8$. The changes in the flow mode and structure behind the cylinder lead to a kink in the curve for the mean lift coefficient. For $\alpha \geqslant 5.15$ the flow was found to be steady state. The lift coefficient again shows a linear increase, converging asymptotically towards the curve based on the potential flow theory combined with the asymptotic approximation of Moore[5] to determine the circulation Γ.

In order to obtain more detailed information about this phenomenon for a wide parameter range, additional numerical simulations of the two-dimensional unsteady laminar

[a]Author to whom correspondence should be addressed. Electronic mail: breuer@lstm.uni-erlangen.de

flow past a rotating circular cylinder for Re=60, 80, 160, and 200 and $0 \leqslant \alpha \leqslant 6$ were performed.

II. COMPUTATIONAL METHODOLOGY

The standard set of partial differential equations, consisting of the continuity and the momentum equations in nondimensional form, was considered. This set of equations has to be solved for the unknown pressure p, and the two velocities u_i for $i=1,2$ in the x and y directions. The influence of gravity force was excluded from the present considerations. Because the energy equation is decoupled from the system of other conservation equations, it was not taken into account.

The computations were carried out with the highly efficient flow simulation code *LESOCC*, based on the finite-volume method for arbitrary nonorthogonal, body-fitted, nonstaggered grids (see Breuer[6,7]). Convection and diffusion terms in the momentum equations are approximated by central differencing scheme of second-order accuracy. A low-storage multistage Runge–Kutta method (three substeps, second-order accurate in time) is applied to integrate the momentum equations in the predictor step. Within the corrector step the Poisson equation for the pressure correction is solved implicitly by the incomplete LU decomposition method of Stone.[8]

In the present study, an O-type grid was used with an outer boundary of diameter H and an inner boundary on the cylinder surface, $D/2$. The classical far-field boundary conditions were used. The size of the domain for all predictions was $H/D=100$, which was proved to be sufficiently large by additional predictions using domain sizes of up to $H/D=300$. The number of grid points in radial and circumferential direction was 241×241 and all other parameters concerning the quality of the grid correspond to those already used in the calculation of Kang *et al.*[3] Furthermore, this grid and the *LESOCC* code were used to confirm the results for Re=100 and $\alpha=5$ reported by Stojković *et al.*[1]

III. RESULTS AND DISCUSSION

The numerical results obtained clearly confirm the existence of the second shedding mode in the Reynolds number range investigated. The interval $\alpha_{\mathrm{II}} \leqslant \alpha \leqslant \alpha_{\mathrm{III}}$ in which the second vortex shedding mode appears is significantly narrower than that defining the first shedding mode ($0 \leqslant \alpha \leqslant \alpha_{\mathrm{I}}$), as visible in the stability diagram in Fig. 1. The critical rotational speeds defining these two vortex regions for Re=60, 80, 100, 160, and 200 are $\alpha_{\mathrm{I}}=1.4$, 1.7, 1.8, 1.9, and 1.9, $\alpha_{\mathrm{II}}=5.35$, 5.0, 4.8, 4.5, and 4.35, and $\alpha_{\mathrm{III}}=5.45$, 5.2, 5.1, 4.8, and 4.6, respectively. For each Re investigated, successive computations with an incrementally increasing and decreasing rotation rate ($\Delta\alpha=0.05$) were carried out around the critical values leading to the bifurcation curves in Fig. 1. Using a much finer grid than in the previous study,[1] a slightly different value for α_{III} is observed at Re=100. Based on the bifurcation diagram in Fig. 1, it is obvious that α_{I} increases monotonically with increasing Re. Kang *et al.*[3] found a logarithmic increase of α_{I} with increasing Re. However, based on the present data, it was neither possible to prove nor to disprove this statement. Contrarily, both curves for α_{II} and α_{III} decrease with increasing Re.

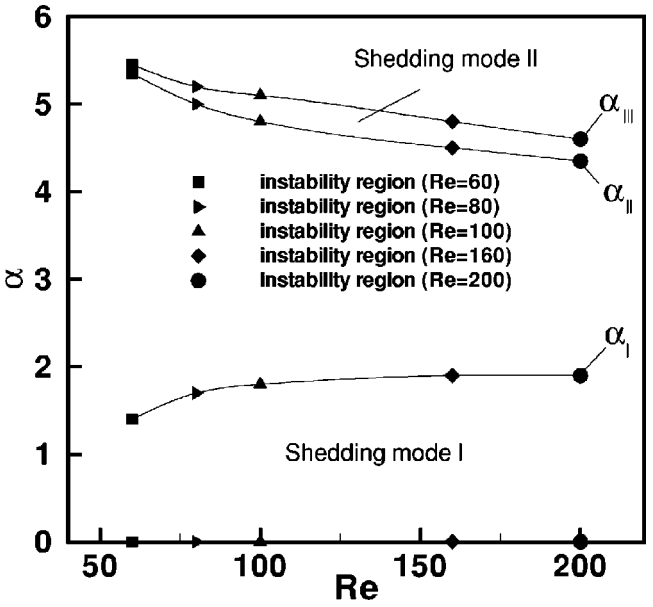

FIG. 1. Stability diagram for different Reynolds numbers $60 \leqslant \mathrm{Re} \leqslant 200$ and rotation rates $0 \leqslant \alpha \leqslant 6$.

The variation of the Strouhal number $\mathrm{St}=fD/U_\infty$ for $60 \leqslant \mathrm{Re} \leqslant 200$ and $\alpha_{II} \leqslant \alpha \leqslant \alpha_{\mathrm{III}}$ is shown in Fig. 2, where f denotes the vortex shedding frequency. In order to compare these St values with the corresponding values of the first vortex shedding region $0 \leqslant \alpha \leqslant \alpha_{\mathrm{I}}$, the St data for $\alpha=1$ are included in the figure. According to these results, the unsteady flow motion found in the second vortex shedding regime (see Fig. 1) is characterized by a frequency much lower

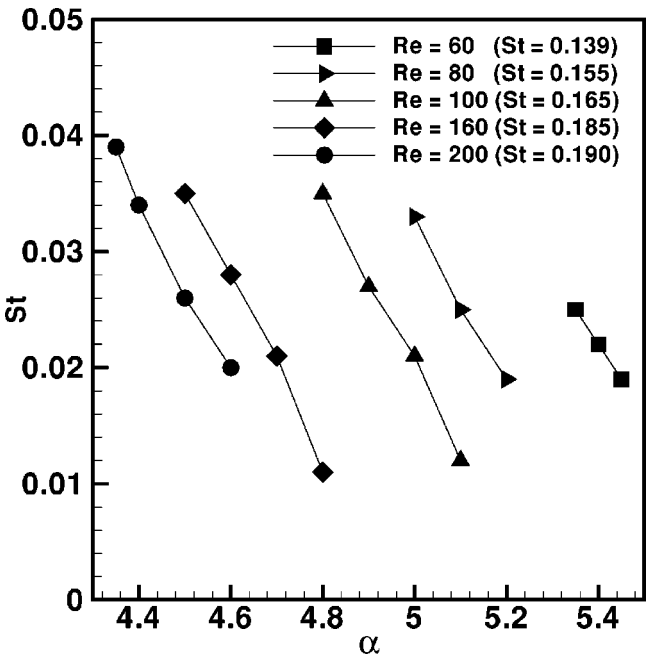

FIG. 2. Strouhal number St versus rotation rate α at Re=60, 80, 100, 160, and 200. The values in parentheses are the Strouhal numbers for $\alpha=1$.

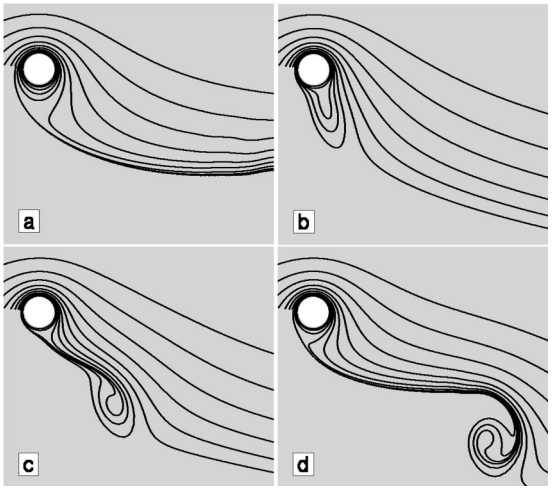

FIG. 3. Development of the vortex street in the second vortex shedding mode behind the rotating cylinder for Re=160 and $\alpha=4.7$.

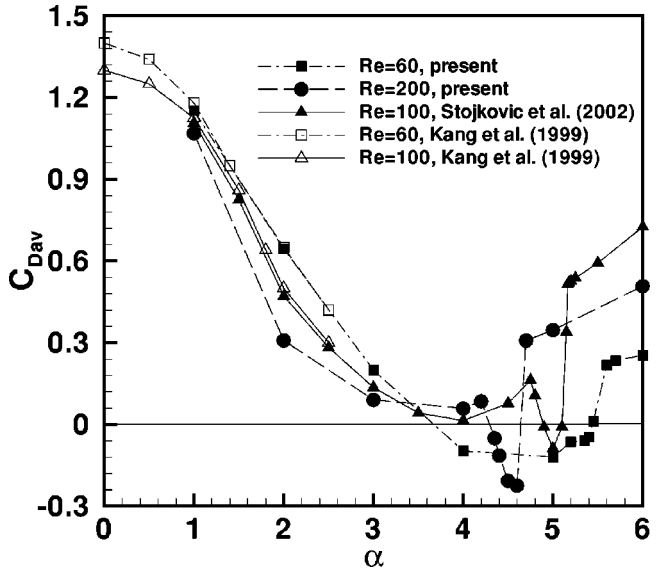

FIG. 4. Mean drag coefficient c_{Dav} for Re=60, 100, and 200 and $0\leqslant\alpha\leqslant6$.

than that of the first shedding mode. Furthermore, the Strouhal number dependence on α in the second vortex shedding mode is much stronger than that characterizing the first mode. With increasing rotation rates, St substantially decreases for each Re investigated. In the case of Re=160, St($\alpha=\alpha_{\mathrm{III}}$) is approximately three times lower than St($\alpha=\alpha_{\mathrm{II}}$). It is worth to mention that the slope of the different St(α) curves is nearly independent of Re. Due to insufficient data points it was, however, not possible to find an appropriate fitting curve characterizing the behavior of St with respect to α and Re.

The development of the vortex street behind the rotating cylinder in the second mode is visualized by computed streaklines shown in Figs. 3(a)–3(d) exemplarily for Re=160 and $\alpha=4.7$. The cylinder rotating in the clockwise direction is exposed to free-stream flow coming from the left. Owing to rotation and strong viscous effects near the cylinder, an egg-shaped region of closed streaklines [see Fig. 3(a)] is formed around the cylinder (also visible from streamlines as shown by Stojković *et al.*[1]). This structure increases in time. The oncoming fluid flow from the lower part of the cylinder forces this egg-shaped region to elongate, see Figs. 3(b) and 3(c). After the egg-shaped structure has reached a certain size, the structure detaches from the cylinder as visible in Fig. 3(d), and the entire process starts anew. As is obvious from Fig. 3, the entire process of vortex formation and shedding is completely different to that characterizing the nonrotating cylinder. Only one vortex appears and develops below the cylinder and not two of them which typically appear behind the nonrotating cylinder developing and detaching from the body in an alternating manner. Furthermore, the time scales of both shedding motions are completely different. Whereas for the classical shedding mode around slowly rotating cylinders the ratio of the time periods for one shedding cycle and a complete revolution of the cylinder is of the order $\mathcal{O}(1)$, the complete cycle for the second shedding mode persists for a multitude of cylinder revolutions, e.g., about 71 for the case displayed in Fig. 3.

Figure 4 shows the dependence of the mean drag coefficient for Re=60, 100, and 200 and $0\leqslant\alpha\leqslant6$. The results for low rotational rates and Re=60 and 100 are consistent with the results obtained by Kang *et al.*[3] for $\alpha\leqslant\alpha_{\mathrm{I}}$, i.e., in the first shedding regime. As can be seen in Fig. 4, the behavior of the drag coefficient can be split into three characteristic regions. For $\alpha\leqslant\alpha_{\mathrm{II}}$ the mean drag coefficient c_{Dav} decreases with increasing rotation rate. In the vicinity of the α interval for the second vortex shedding mode c_{Dav} starts to increase (see, e.g., Re=100) but then abruptly drops, leading to a kink in the c_{Dav} curve. This phenomenon is pronounced for Re=100 and 200 but not so clearly visible for Re=60. The sudden drop of c_{Dav} results in negative values of the mean drag coefficient which is equivalent to thrust. With increasing Re the kink becomes more pronounced and appears for smaller α values. This kink in the c_{Dav} curve indicates that the flow mode and structure behind the cylinder has changed and the second vortex shedding has started. However, by further increasing the rotational rate to $\alpha>\alpha_{\mathrm{III}}$, the flow is stable and steady again and c_{Dav} continues to increase smoothly. In spite of this increase of c_{Dav} within this region, it was shown by Stojković *et al.*[1] that the corresponding flow field is very similar to the structure known from potential theory. In contrast the flow structure for $\alpha_{\mathrm{I}}<\alpha<\alpha_{\mathrm{II}}$ strongly deviates from the solution of potential theory. Hence it was found that the flow within the region $\alpha_{\mathrm{II}}\leqslant\alpha\leqslant\alpha_{\mathrm{III}}$ toggles between two characteristic flow structures, one for $\alpha\leqslant\alpha_{\mathrm{II}}$ where the viscous effects are very important and the other for $\alpha\geqslant\alpha_{\mathrm{III}}$ where the viscous effects are mainly restricted to the vicinity of the cylinder and the rotation dominates the entire flow, leading to a flow structure very similar to the potential flow field. This explains why for increasing Re the second vortex shedding mode appears for smaller values of α. Actually, Re could be considered as the ratio of inertial and viscous forces and with increasing Re the viscous effects are not so dominant in the flow field and thus the rotational rates, causing the potential flow field structure, do not have to be as high as for the case of smaller Re.

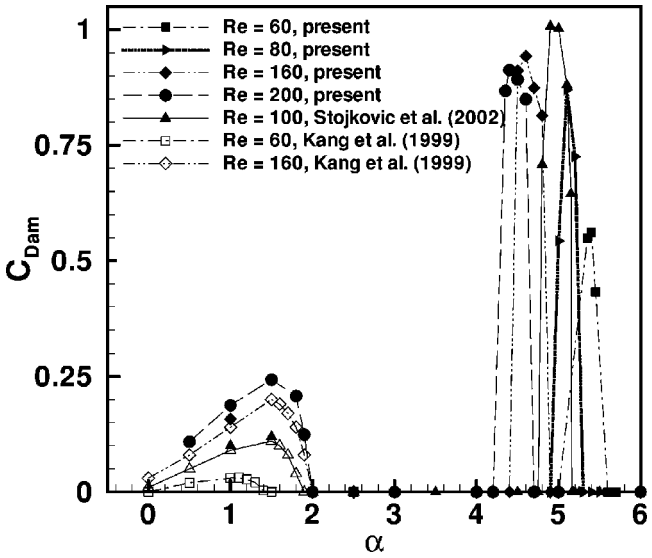

FIG. 5. Amplitude of the drag coefficient c_{Dam} for Re=60, 80, 100, 160, and 200 and $0 \leqslant \alpha \leqslant 6$.

Because nonsinusoidal histories of the drag and lift coefficients were observed in the second vortex shedding mode, the amplitude is defined in a general way by $c_{Dam} = 1/2(c_{D\max} - c_{D\min})$ and corresponding results are presented in Fig. 5. This figure clearly confirms that the first vortex shedding mode appears at low rotational rates $\alpha < \alpha_{\mathrm{I}}$ and then completely disappears for $\alpha_{\mathrm{I}} \leqslant \alpha \leqslant \alpha_{\mathrm{II}}$. The results for lower rotational rates produced by Kang *et al.*[3] are included in the figure, coinciding well with the corresponding results of the present calculation. For $\alpha < \alpha_{\mathrm{I}}$ the amplitude of the drag coefficient c_{Dam} increases almost linearly with increasing α and sharply reduces to zero for $\alpha \geqslant \alpha_{\mathrm{I}}$. Furthermore, with increasing Re at $\alpha = \text{const.}$, c_{Dam} increases for the first shedding mode. The second vortex shedding mode takes place for $\alpha_{\mathrm{II}} \leqslant \alpha \leqslant \alpha_{\mathrm{III}}$. The amplitude of the drag signal in this mode shown in Fig. 5 is up to four times higher than those characterizing the first shedding mode for the same Re investigated. It was also observed that the amplitude of the lift coefficient (not shown here) is approximately 25% higher than the corresponding amplitude of the drag coefficient for the same Re and α within $\alpha_{\mathrm{II}} \leqslant \alpha \leqslant \alpha_{\mathrm{III}}$. For $\alpha \geqslant \alpha_{\mathrm{III}}$ the flow is again stable, showing no kind of shedding motion.

IV. CONCLUSIONS

It is concluded that for all Reynolds numbers characterizing a two-dimensional laminar unsteady flow, the second vortex shedding mode exists for the flow around a rotating cylinder. The second mode appears in the range $4.35 \leqslant \alpha \leqslant 5.45$ depending on Re. This vortex shedding mode is characterized by a frequency much lower than that characterizing the classical von Kármán vortex shedding. Furthermore, St is strongly dependent on the rotational rate and weakly dependent on the Reynolds number: with increasing α the frequency of the shedding substantially decreases, whereas an increasing Re at fixed α leads to slightly lower frequencies. Additionally, the amplitudes of the fluctuating lift and drag coefficient are much higher for the second shedding mode than those known for the first mode around a nonrotating or slowly rotating cylinder. The mean drag coefficient is found to strongly depend on the rotational rate α leading to negative values (thrust) within the second shedding mode. Furthermore, it was observed that with increasing Re the second shedding mode appears for smaller values of α. This could be attributed to a smaller influence of the viscous forces when Re is increased.

[1] D. Stojkovic, M. Breuer, and F. Durst, "Effect of high rotation rates on the laminar flow around a circular cylinder," Phys. Fluids **14**, 3160 (2002).
[2] M. M. Zdravkovich, *Flow Around Circular Cylinders, Vol. 1: Fundamentals* (Oxford University Press, New York, 1997).
[3] S. Kang, H. Choi, and S. Lee, "Laminar flow past a rotating circular cylinder," Phys. Fluids **11**, 3312 (1999).
[4] H. M. Badr, S. C. R. Dennis, and P. J. S. Young, "Steady and unsteady flow past a rotating cylinder at low Reynolds numbers," Comput. Fluids **17**, 579 (1989).
[5] D. W. Moore, "The flow past a rapidly rotating circular cylinder in an infinite stream," J. Fluid Mech. **2**, 541 (1957).
[6] M. Breuer, "Large-eddy simulation of the sub-critical flow past a circular cylinder: Numerical and modeling aspects," Int. J. Numer. Methods Fluids **28**, 1281 (1998).
[7] M. Breuer, "A challenging test case for large-eddy simulation: High Reynolds number circular cylinder flow," Int. J. Heat Fluid Flow **21**, 648 (2000).
[8] H. L. Stone, "Iterative solution of implicit approximations of multidimensional partial differential equations," SIAM (Soc. Ind. Appl. Math.) J. Numer. Anal. **5**, 530 (1968).